Nano Energy 81 (2021) 105617

Contents lists available at ScienceDirect

Nano Energy

journal homepage: http://www.elsevier.com/locate/nanoen

Biomimetic underwater self-perceptive actuating soft system based on highly compliant, morphable and conductive sandwiched thin films

Yun Liang [a,b], Peng Xiao [a,b,*], Feng Ni [a,b], Ling Zhang [a], Tao Zhang [a,b,*], Shuai Wang [a], Wei Zhou [a,b], Wei Lu [a,b], Shiao-Wei Kuo [c], Tao Chen [a,b,*]

[a] Key Laboratory of Marine Materials and Related Technologies, Zhejiang Key Laboratory of Marine Materials and Protective Technologies, Ningbo Institute of Materials Technology and Engineering, Chinese Academy of Sciences, Zhongguan West Road 1219, 315201 Ningbo, China
[b] School of Chemical Sciences, University of Chinese Academy of Science, Beijing 100049, China
[c] Department of Material and Optoelectronic Science, Center of Crystal Research, National Sun Yat-Sen University, Kaohsiung 804, Taiwan

ARTICLE INFO

Keywords:
Conformal conductive films
Morphable
Water-repellent
Pneumatic actuator
Synergetic perceptive and actuating systems

ABSTRACT

In biological system, autonomic neural perception and motion behaviors enable adaptive capability to the external environments. The biomimetic construction of soft materials with synergetic perceptive and actuating characteristics that is highly desirable for realizing the intelligent soft systems. Also, current prototypes do not provide appropriate platforms for the closeup exploration of underwater life in a safely and silently interactive way. Here, we have developed a compliant, morphable and conductive sandwiched film composed of carbon nanotubes (CNTs) film sandwiched between two polydimethylsiloxane (PDMS) layers that can function as a self-perceptive soft actuator. The vertical movement of the actuator can be accurately controlled by applying extra pressure, which attributed to the deformation of elastic ultrathin PDMS film like the swim bladder. Furthermore, the actuator can real-time traced the actuation process and sensing the surrounding environment by composite a layer of CNTs film, also realized to guide the motions of the actuator according to the feedback signals.

1. Introduction

Biological creatures can survive and prosper in complicated nature environment, owing to their excellent adaptive capabilities to perceive dangerous signals and adjusting their morphology, phenotype and physiology accordingly. One of the most important component of these bio-systems is the soft tissue integrated with perceptive and mechanically deformable features to reversibly change their appearance and behaviors [1,2]. Inspired by these desirable capabilities, extensive efforts have been devoted to exploit various soft materials to realize colorimetric sensors/actuators [3–9], electronic skins [10–16] and pneumatic/hydraulic driven camouflage systems [17–20]. As a promising bionic candidate of soft materials, silicone-based elastomer that are intrinsically flexible, stretchable and compliant, can well mimic natural systems and functions in an environment-friendly way [2,21–24].

To date, diverse functional components have been integrated into elastomers to endow them with designable morphology and functionality to achieve bionic and soft robotics with organism-like behaviors [6,12,25–30]. Recently, Shepherd et al. reported a typical example that the alternative introduction of inextensible textile patterns into elastomeric membrane to achieve controllable shape-transformation from two-dimensional (2D) planar surface to three-dimensional (3D) non-Euclidean shapes [18]. In another system, Gorodetsky et al. developed a sandwiched acrylate elastomer, that incorporated with proton-conducting component, could dynamically modulate light propagation via mechanical or electrical actuation, promising for stretchable cephalopod-like camouflage [31]. Although the skin-like stretchable morphing behaviors with variation forms have been explored in elastomer-based actuating systems, the lack of synergetic sensory and deformable/locomotive features in one system may cause poor controllability of closed-loop as well as weak response to external stimuli [28,32,33]. Beyond the land environments, there also remains a fascinating and emerging regime of subaqueous bionic intelligent behaviors that are unexploited in an artificial integrated system [34,35]. Nature has provided us unique perceptive for subaqueous intelligent system. For example, the swim bladder of clownfish functions as a resonator to perceive the environment and further guide reversible inflation and deflation behavior to control vertical motion in water

* Corresponding authors at: Key Laboratory of Marine Materials and Related Technologies, Zhejiang Key Laboratory of Marine Materials and Protective Technologies, Ningbo Institute of Materials Technology and Engineering, Chinese Academy of Sciences, Zhongguan West Road 1219, 315201 Ningbo, China.
E-mail addresses: xiaopeng@nimte.ac.cn (P. Xiao), tzhang@nimte.ac.cn (T. Zhang), tao.chen@nimte.ac.cn (T. Chen).

https://doi.org/10.1016/j.nanoen.2020.105617
Received 22 July 2020; Received in revised form 6 November 2020; Accepted 15 November 2020
Available online 19 November 2020

[36–39]. The abilities to recognize, adapt, behave and further share information underwater can help to discover new objects and enrich the limited map in novel situations [40–42].

Inspired by the actuating and sensory principle of swim bladders, in this work, we show the design and fabrication of a soft and elastic underwater integrated actuating and sensory hybrid film. The film is based on a conformal sandwiched structure composed of stretchable elastic PDMS matrix and conductive CNTs film, which can be further integrated into a hollow system for a self-supported system. Owing to the favorable shape-adaptable and morphable features of the film, it can achieve a controllable underwater up/down motion via an inflation/deflation strategy. Based on a piezoresistive sensing mechanism, the stretchable deformation of the film can directly adjust the conductive CNTs network to realize a real-time and stable underwater sensory capability. Moreover, the self-supported film can further capture the external vibration signals mediated by the water vibration transmission. As a result, the sensing and actuating functions can be effectively integrated into one sandwiched film for synergetic biomimetic behaviors. As a proof-of-concept, an artificial swim bladder anchored on a fish model is developed to actively capture the vibration stimuli and perform a pneumatic actuation, demonstrating significant potentials in intelligent integrated soft robotics.

2. Results and discussion

Benefitting from the swim bladder, clownfish are capable of perceiving the ambient environment and then making the responding decision of locomotion control through the bladder's reversible inflation

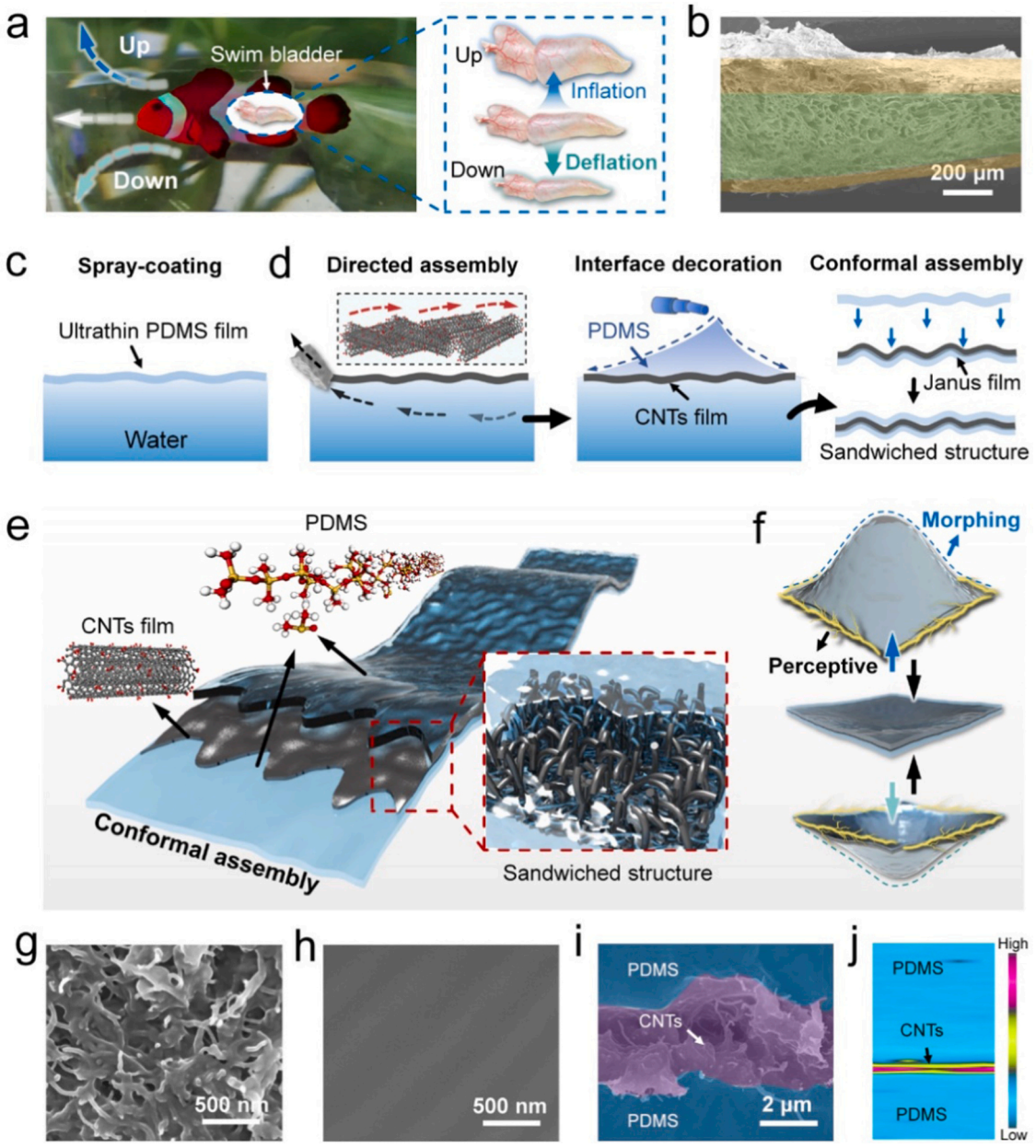

Fig. 1. (a) A photo of a clownfish and the schematic illustration of the surfacing/diving motion driven by inflating/deflating the swim bladder. (b) SEM image of a real swim bladder after freeze-drying. Schematic illustration of the fabrication process of the ultrathin PDMS film (c) and CNTs/PDMS Janus film at air/water interface and conformal sandwiched integrate into a sandwiched self-perceptive morphing film (d). (e-f) Schematic illustration of the conformal self-perceptive morphing PCP film. SEM images of the CNTs/PDMS Janus film at water side layer with plenty of exposed CNT (g) and with a smooth surface at air side (h). Cross-sectional SEM image (i) and Raman mapping (j) of the PCP film.

and deflation (Fig. 1a). To imitate the form and function principle of the swim bladder (Fig. 1b) [43], a sandwich-structured film was prepared by conformally integrating a Janus CNTs/PDMS film and a PDMS film through a simple but effective method at the water/air interface. Firstly, the ultrathin PDMS film was achieved on the other air/water interface by spraying technique, which is self-adhesive and appropriated for encapsulation (Fig. 1c) [44]. Then, the CNTs/PDMS ultrathin Janus hybrid film was fabricated by a typical CNTs self-assembly at the air/-water interface and in-situ interfacial asymmetric decoration of PDMS (Figs 1d and S1) [44,45]. It can be observed clearly that at the water side of the Janus film, CNTs stretch out of the PDMS matrix and ensure the conductive pathways, while the air side shows a smooth surface of PDMS (Fig. 1g and h). This result can be attributed to the immiscibility between PDMS/N-heptane and water. Only the CNTs exposing to the air side can be covered by PDMS as the other side is effectively protected by the water. The asymmetric bilayer structure of the Janus film was further verified by its cross-section images (Fig. S2). It's noticeable that the interlocked structure between CNTs and PDMS can not only significantly improves the robustness of conductivity, but also endows an excellent stretchability by redistributing the strain energy through randomly located CNTs [46]. Due to the excellent electrical and mechanical properties, the CNTs/PDMS hybrid film was used as a perceptive component with a neural-like function. Finally, the sandwiched structure film was constructed by conformally integrating the pure ultrathin PDMS film with CNTs/PDMS Janus film (PCP film) (Fig. 1e) and the thickness is about 60 μm (Fig. S3b). Such a film performs the favorable abilities of underwater non-destructive perception and morphing (Fig. 1f). The cross-section structure of the PCP film was characterized by SEM and Raman mapping (Fig. 1i and j), which indicates an obvious sandwiched structure and good combinative ability between two layers. The structure and functions of the film show high similarity with that of the swim bladder, which indicates a biomimetic artificial swim bladder could be constructed.

To verify the compliance, shape-adaptable and morphing properties of the ultrathin elastic film, the ultrathin PDMS film was conformally transferred onto an open container to form a closed system (artificial swim bladder). When the pressure out of the system was changed, a difference of pressure between inside and outside of the system occurred and causing a significant deformation of the elastic PDMS film (Fig. 2a), which indicates the excellent pneumatic morphing ability. While the system with a proper density was put into the water, a diving/surfacing cycle motion was achieved by adjusting the pressure (Fig. 2b). When the pressure inside the swim bladder is relatively increased by decreasing the air pressure over the water, the swim bladder will be inflated, which will result in additional buoyancy and a surfacing motion of it. Similarly, the diving motion of the system could be control by relatively decreased the inner pressure of it. This phenomenon is similar to the volume change behavior of the swim bladder, which are conducted by deflating/inflating its bladder as well [36].

The correlation between the buoyancy change and the diving/surfacing motions can be explained as follows: the forces of the system mainly include the gravitational force (G), buoyancy (F) and the fluidic resistance (f), where G and f can be regarded as constants at the initial diving/surfacing state, whereas F is dependent on the displacement, which can be adjusted by the morphing of the elastic matrix according to Eq. (1).

$$F = \rho g v \tag{1}$$

Where ρ is the density of the water; g is the gravitational acceleration; v is the volume of the system. When the total density of the actuator larger than that of water, $G > F + f$, without applying extra pressure to the system, the device stayed at the bottom in the beginning. After a

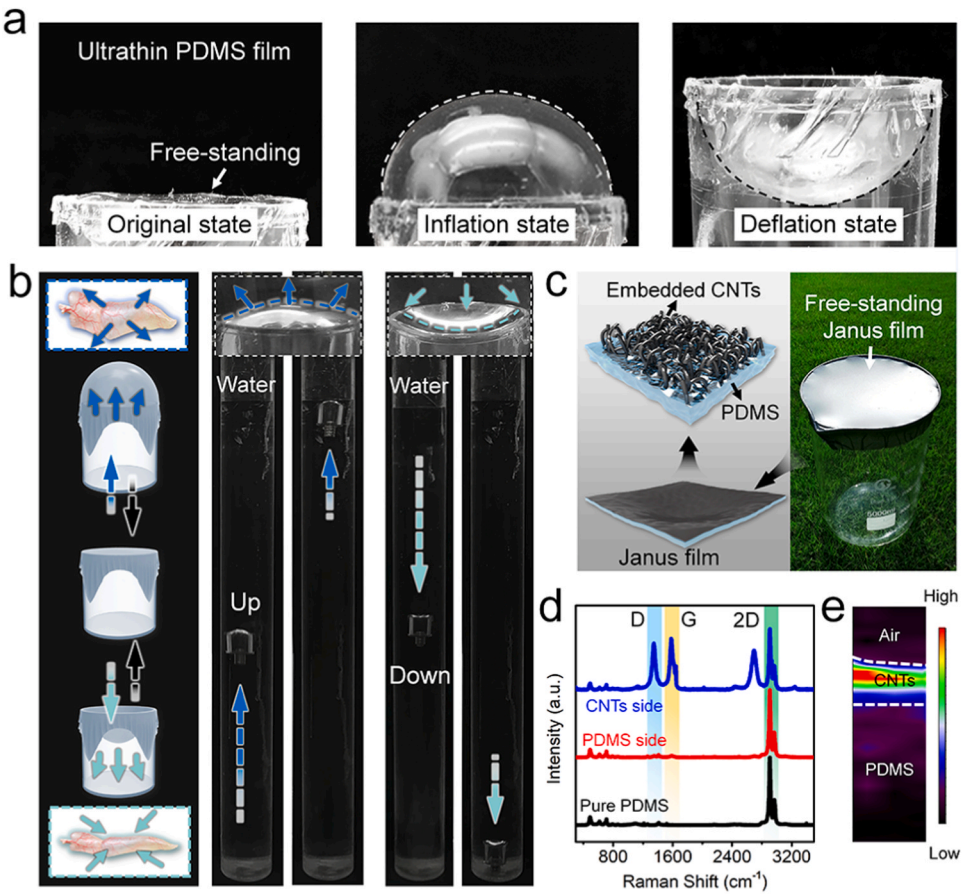

Fig. 2. (a) Photographs of the ultrathin free-standing PDMS film at different states. (b) Illustration of the inflation and deflation morphing of the ultrathin PDMS film to imitate the swim bladder and the time-lapse images of the system during the underwater surfacing/diving process, which caused by inflation and deflation morphing of the PDMS film. (c) Photograph of free-standing CNTs/PDMS ultrathin Janus film on a beaker with embedded structure. (d) Raman spectra of the pure PDMS and both sides of the CNTs/PDMS Janus film. (e) Raman mapping of the cross-sectional of PDMS/CNTs Janus film.

negative pressure (−20 kPa) applied, the device rising to the water surface due to the ultrathin PDMS film outward expansion to increase the volume and F of the system, resulting in F > G + f. As the pressure was released back to the original state, the film recovered to the flat state, where G > F + f and resulting in diving. On the contrary, when the total density of the actuator smaller than that of water (F > G + f), without applying extra pressure to the system, the actuator stayed at the water surface in the beginning. After pressurization to 20 kPa, a diving process caused by the ultrathin PDMS film sunken inward, which causing G > F + f by decreasing the volume of the system. Once the pressure was released to the initial atmospheric pressure, the film returns to the flat state and resulting in resurfacing. This phenomenon demonstrates that the pneumatic morphing behavior of the elastic thin PDMS film can be used to imitate the morphing of that swim bladder and further modulated the vertical diving/surfacing motion.

In addition to providing lift for the fish, the swim bladder is also able to perceive its surrounding environment and then give the inflating/deflating instruction to it. The properties of the ultrathin CNTs/PDMS Janus film, the effective sensing component of our artificial swim bladder is systematically investigated in the first place. As shown in Fig. 2c, the Janus film also remains the excellent compliance and self-supporting properties like the ultrathin PDMS film. The Raman spectra were used to characterize the ingredient of both sides the CNTs/PDMS Janus film (Fig. 2d). The water side of the Janus film presence the characteristic D, G and 2D peaks of CNTs at 1349.6 cm^{-1}, 1580.3 cm^{-1} and 2692.8 cm^{-1}, respectively. While the air side of the Janus film only shows the peaks as the same as pure PDMS film. This asymmetrical structure was further verified by Raman mapping (Fig. 2e) and consistent with the SEM results. The Janus property of the CNTs/PDMS film enabled to output the electrical signals and was used as a perceptive component with the neural-like function.

The sensing performance of Janus film was further characterized, as shown in Fig. 3a, a typical plot for the CNTs/PDMS Janus film-based strain sensor was tested at different loading conditions by the normalized electrical resistance ($\Delta R/R_0$) change:

$$(\Delta R/R_0 = (R - R_0)/R_0) \quad (2)$$

where R represents the real-time resistance and R_0 is the initial resistance at the relaxed state (the Janus film strip with lateral dimensions of 20 mm × 3 mm (length × width)). In the uniaxial tensile tests accompanied by simultaneous resistance measurements, the sensor presents a monotonic curve with three obvious stages. The corresponding gauge factor (GF) is defined as the relative ratio of ($\Delta R/R_0$) to tensile strain (ε), which was calculated according to Eq. (3):

$$\varepsilon = (L - L_0/L_0) \quad (3)$$

where L and L_0 are the film length at the tensile state and the relaxed state, respectively. The GFs were calculated to be 25.42 (ε: < 8%), 16.53

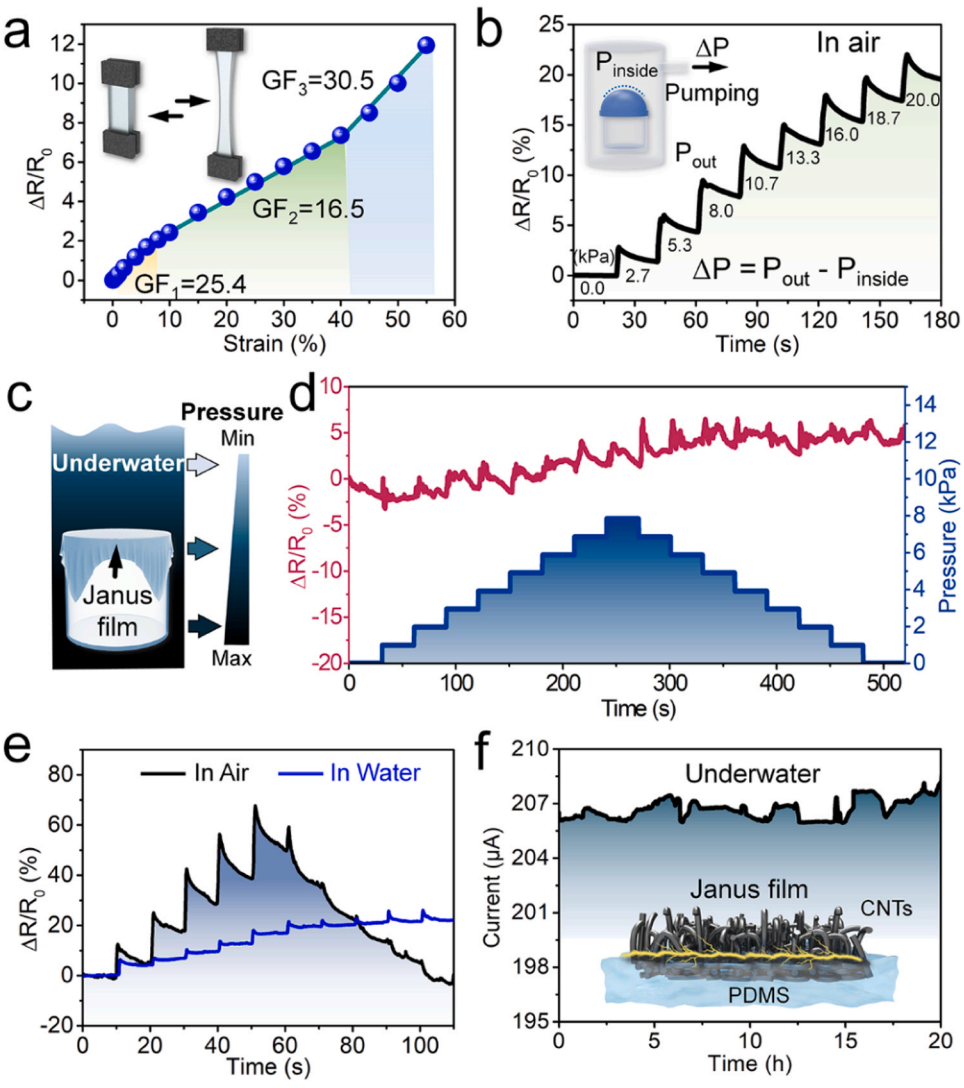

Fig. 3. (a) The sensing performance of the CNTs/PDMS Janus film with a detailed gauge factor. (b) $\Delta R/R_0$ versus time curve of the CNTs/PDMS Janus film when used to construct an artificial swim bladder under different extra pressure in the air. (c) Illustration of the artificial swim bladder with CNTs/PDMS Janus film to sensing the underwater depth. (d) $\Delta R/R_0$ versus time curve of the artificial swim bladder under different water pressure. (e) The resistance change of Janus film sensor during finger bending and releasing behavior both in air and in water. (f) The electrical stability of Janus film underwater.

(ε: 8–40) and 30.49 (ε: 40–55) coupled with a highly linear response were 0.998, 0.996, and 0.990, respectively. Interestingly, when the Janus film is transferred onto a hollow container to construct an artificial swim bladder, the outward expanding morphing of the film can be real-time traced in the air (Figs 3b and S4). While immersed the swim bladder in water, the morphing of the Janus film caused by water pressure at different depths can't be detected efficiently (Fig. 3c and d). Similarly, the bending and releasing behaviors of the finger can be quantitatively monitored with the Janus film attached to the finger surface. However, after immersing the finger into the water, the bending and releasing behaviors can't be monitored efficiently (Figs 3e and S5). The reason for this phenomenon may be explained as follows: when the Janus film immersed in the water, the water and electrolyte molecules penetrate the conductive CNTs network, causing the conductive pathway change and irregular electrical signal change. To verify this conjecture, the electrical stability of the Janus film was tested underwater. As depicted in Fig. 3f, the current value presents a very large fluctuation, which proves that the aqueous solution greatly affects the stability and reliability of the sensor. Therefore, an effective encapsulation of Janus film is inevitable to realize reliable underwater detection for external signals.

Furthermore, the Janus film was sealed via conformal sandwiched integrating with a pure ultrathin PDMS film at CNTs side. As a result, the assembled sandwiched film can be easily achieved in a large-scale and homogenous feature (Figs 4a and S3a). As depicted in Fig. 4b, the PCP film also remained the excellent self-adaptiveness and deformation ability under the extra pressure driving. In contrast to the Janus CNTs/PDMS film, the PCP film performs high electrical stability with water exposure even thoroughly immersed it in water for more than 20 h (Fig. 4c). As a result, the PCP sensor exhibits a constant conductivity (Fig. 4d). It is noteworthy that, even the CNTs film is located in the middle part of the sandwiched films, the stretchable PDMS can still induce the change of contact resistance among CNTs. This mechanism can be evaluated using the 3D fiber reorientation model and affine transformation [47–49]. Thus, the resistance will periodically change during stretch/release cycles. As depicted in Fig. 4e, the sensing performance of the PCP film is similar to the Janus film with three distinct stages. The corresponding gauge factors for these regions are 9.58 ($0 < \varepsilon < 6\%$), 3.77 ($6 < \varepsilon < 25\%$), and 8.18 ($25 < \varepsilon < 55\%$), with the linearities 0.994, 0.995, and 0.990, respectively. The real-time variation of the resistance under repetitive stretching (with ε of 1%, 5%, 10%, 20%, 30% to 40%) shows the stable and continuous responses (Fig. S6). The response of the PCP based sensor toward different frequencies was also investigated (Fig. 4f). Note that the output electrical signals of amplitude remain stable without an obvious change at typical frequencies from 0.01 to 1 Hz, demonstrating the sensor a high reproducibility towards various frequencies. Moreover, bending/release motions of the finger could be accurately recorded by the PCP film sensor both in the air or underwater (Fig. 4g and h). When comparing with other similar strain sensors with the encapsulated structure in previous reports, the PCP sensor presents relatively high sensitivity, excellent stretchability and ultrathin thickness simultaneously (Fig. 4i and Table S1) [47,48,50–59]. Based on those results, we consider the stretchable conductive composite film with sandwiched-structured is of

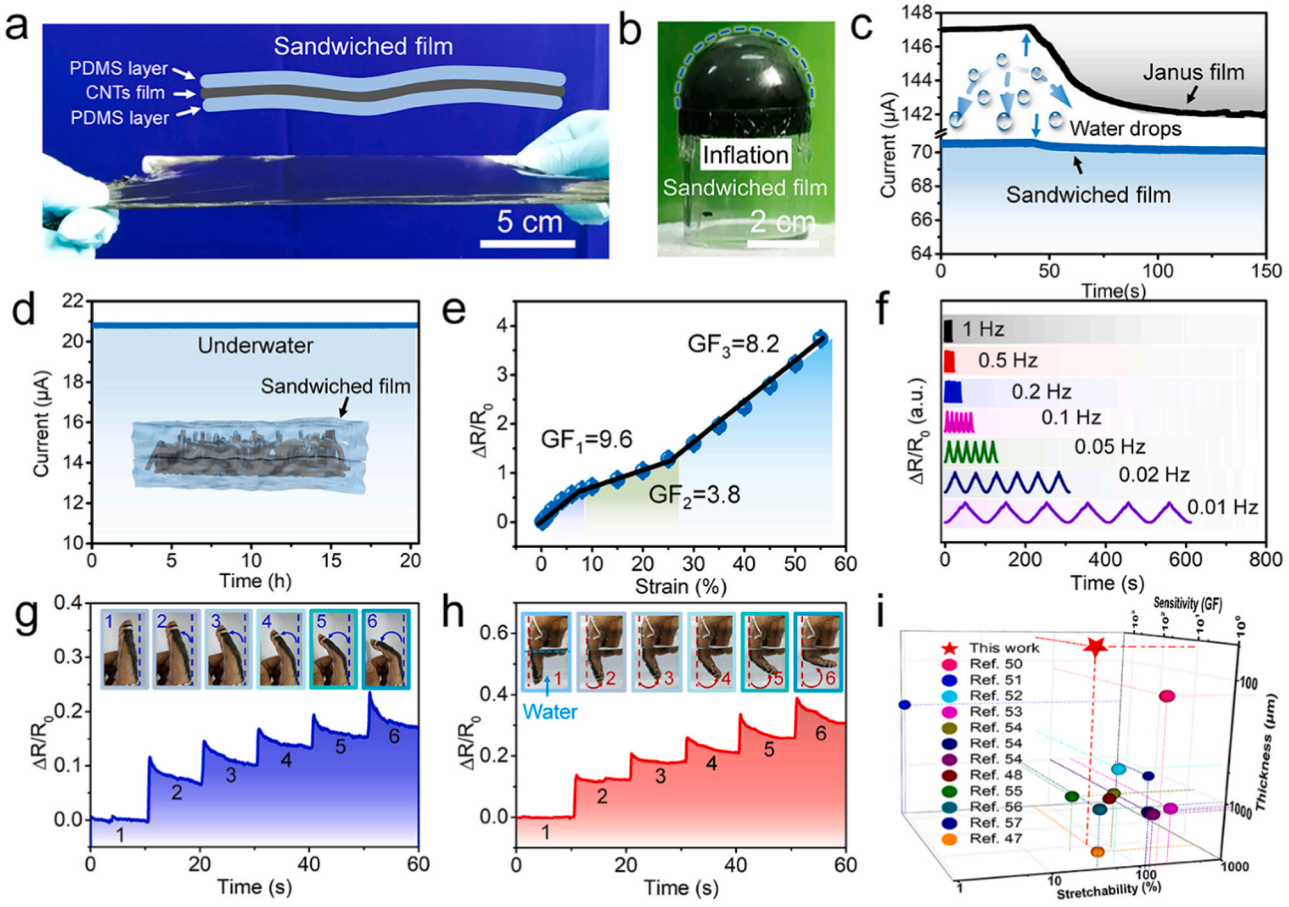

Fig. 4. (a) Photograph of the PCP film, insert: illustration the microstructure of the PCP film. (b) Photograph of a PCP film at inflation state. (c) Electrical stability of the Janus film and PCP film after being dropped with water. (d) The electrical stability of the PCP film when immersed underwater. (e) The sensing performance of the PCP film with detailed gauge factor. (f) Relative resistance variation of the PCP film under different frequencies (from 0.02 to 1 Hz) between 0% and 20% strain. $\Delta R/R_0$ versus time curve of PCP strain sensor during finger bending and releasing behavior in air (g) and water (h), respectively. (i) Comparison of sensitivity (GF), stretchability and thickness between our PCP film sensor and other sandwiched structure sensors in previous works.

reproducible and reliable sensing performance both in air and underwater, which could be applied and integrated into our artificial swim bladder.

Additionally, the deformation performance of the PCP film was further quantitatively characterized through the central angle. For example, the central angles of a film with 36 mm actuation diameter show an excellent linear relationship with the different ambient pressure (from 0 to 20 kPa), which also presents excellent consistency with the finite element simulation results (Fig. 5a–c). Furthermore, to verify the universalistic actuation performance, the central angles of a serious of PCP films with different actuation diameters were characterized by finite element simulation under 20 kPa, which all result in about 120° (Figs 5d and S7). The above results indicate that our PCP film can be used to construct actuators at any scales, and the actuation performance

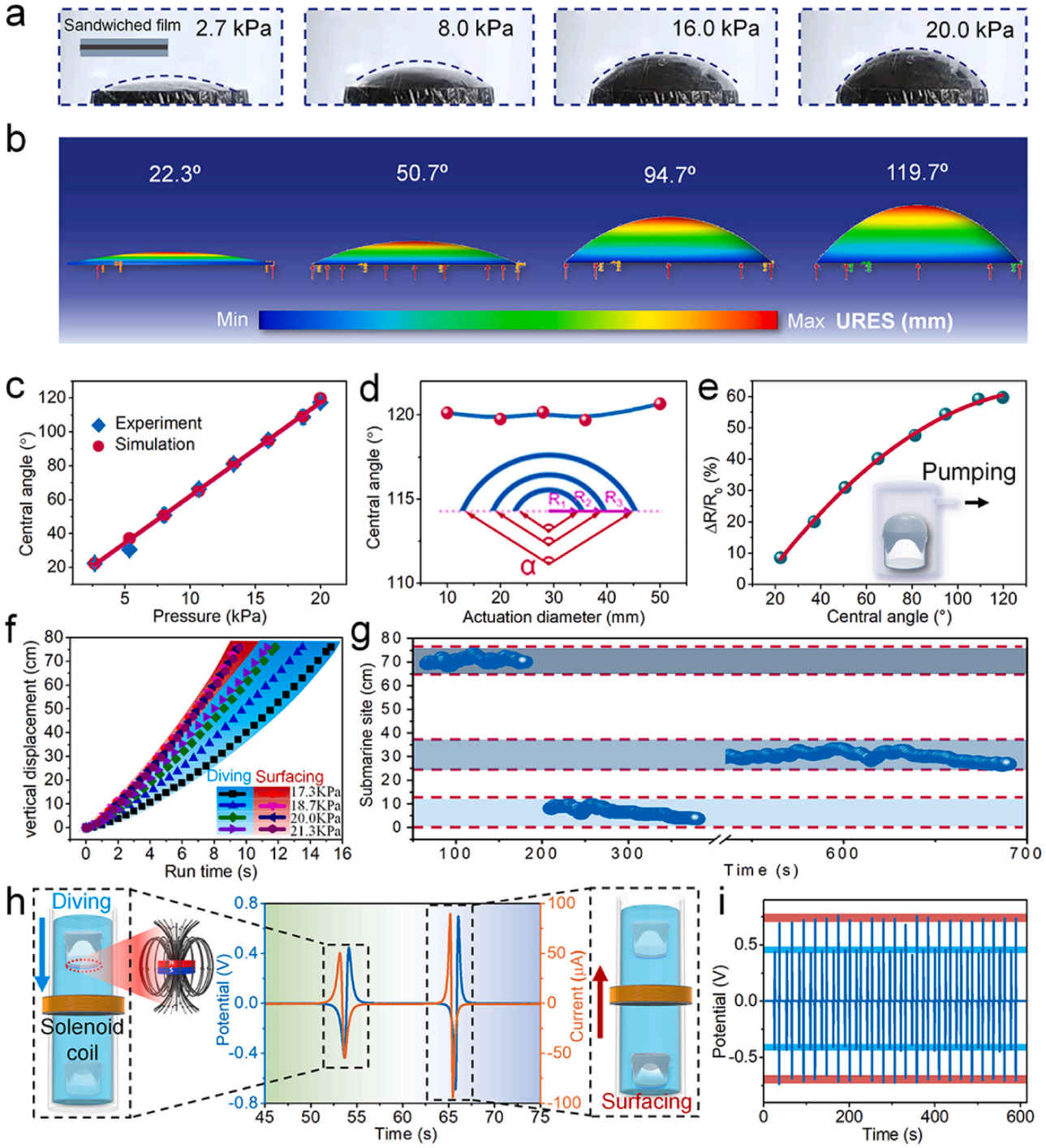

Fig. 5. (a) The deformation performance of the PCP film at different ambient pressures with actuation diameter of 36 mm. (b) Finite element simulation the deformation performance of the PCP film at the corresponding condition. (c) Central angle curves in responding to various ambient pressures with experimental and finite element simulation results. (d) Finite element simulation results at the 20 kPa with different actuation diameters (10, 20, 28, 36 and 50 mm). (e) $\Delta R/R_0$ versus central angle curve of the PCP based pneumatic actuator. (f) The diving velocity and surfacing velocity (In terms of displacement and time) of the pneumatic actuator at different extra pressures. (d) Plots of height versus time to describe the suspension ability of the pneumatic actuator by controlling ambient pressures. (h) Potential and current generated by cutting the magnetic induction line curve during a diving and surfacing cycle. (i) The corresponding potential-time curves for the cycled diving-surfacing process at the extra pressure of 17.3 kPa.

has good predictability.

Meanwhile, the electrical signal during the pneumatic morphing was also recorded as shown in Fig. 5e and Fig. S8 of the Supporting Information. It can be observed that with the increase of the pressure and central angle, the $\Delta R/R_0$ value increases monotonously. This indicates that the deformation of the actuator during the pneumatic actuation can be real-time tracked and detected by the electrical signal, thus avoiding the traditional disadvantage of tracking its driving ability by post-processing digital camera photos [60]. It shows the potential as a self-perception actuator to sense and respond to external signals.

Similarly, when the pneumatic actuation system was put into water and then covered with a thin PDMS film to separate the water from the air phase, an artificial swim bladder with water-repellent self-perceptive property can be constructed. When the pressure out of the system was changed, a significant deformation of the PCP film occurred, which results in a diving/surfacing motion. Moreover, the motion velocity of the actuator can be adjusted by extra pressure. The maximal diving and surfacing velocity reached 8.4 cm s^{-1} and 10 cm s^{-1} in our experiment, this corresponds to 4.2 and 5 times its body length per second (Figs 5f and S9). The suspension ability of the actuator was further described by height and velocity through pressure controlling. The height oscillation of the actuator can be confined anywhere, such as at 0–14 cm, 25–37 cm and 65–76 cm, respectively (Fig. 5g). While the vertical velocity was modulated between -0.7 and 0.8 cm s^{-1} (Fig. S10). The above evidence demonstrates that the motion of the actuator can be accurately controlled by controlling the morphing of the film through extra pressure.

Furthermore, the diving/surfacing process of the actuator indicates the potential application of conversion of the kinetic energy into electrical energy by applying Faraday's law (Fig. 5h). A copper coil (10k turns) was fixed in the middle of the container and connect with electrochemical workstation to collect and record the electric generation. A typical voltage and current output profile obtained during a diving/surfacing cycle motion (Fig. 5h). The first two peaks corresponding to the diving process, when the actuator load with magnet gradually approached the coil from the top of the tube container, which results in a magnetic flux increase and an induced negative voltage and the positive current was recorded. After the magnetic flux reached the maximum and the actuator across the coil, the magnetic flux decrease, which results in another opposite induced potential and current with a bigger value, because the velocity of the actuator became larger according to the correlation of $E = Bl\nu$ (E: induced voltage; B: magnetic induction intensity; l and ν: size and velocity of the device) [61]. As the surfacing process, the signal profile was recorded with two similar and bigger signal spikes, this is due to the rising rate is larger than that of diving. Under these conditions, the sustainable energy conversion and steady electricity output of the system were further investigated by recording a potential-time and current-time curve. As shown in Fig. 5i and Fig. S11a

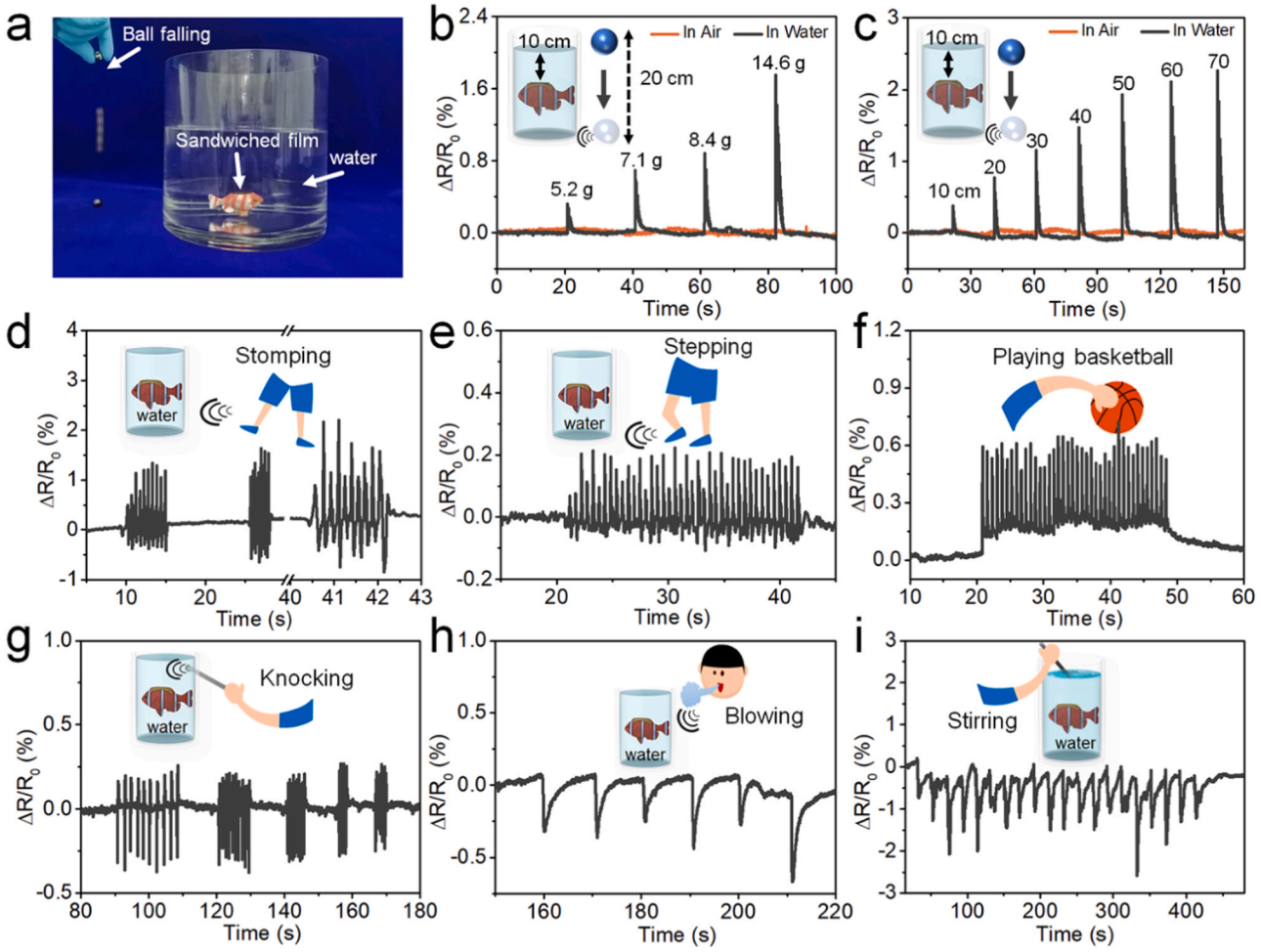

Fig. 6. (a) Illustration of the artificial swim bladder to sense the surrounding environment in a non-touching way. (b) $\Delta R/R_0$ versus time curves of the artificial swim bladder (placed 10 cm underwater and in air, respectively) when stimulated by falling balls with different weights but the same height of 20 cm. (c) $\Delta R/R_0$ versus time curve of the artificial swim bladder (placed 10 cm underwater and in air, respectively) when stimulated by falling balls (8.4 g) with different weights. Responses of the artificial swim bladder to human stomping (d), human stepping (e), playing basketball (f), knocking water container by a ruler (g), blowing air (h) and ruler sliding (i).

in Supporting information, both the positive and negative induced voltage and current values remained constant at a high level, indicating that the morphing of the PCP film and reciprocating motions of the actuator are robust with a long lifetime and that the electricity generation is sustainable. Additionally, the induced potential and current value can be adjusted by applying extra pressure (Fig. S11b and c). Thus, this pneumatic underwater actuator based mini-generator also providing the potential for uses of micromachine systems even in situ power generation in implanted cardiac pacemakers [62].

To explore the sensing ability of our bladder, it was placed in a simulated environment of 20 cm underwater (Fig. 6a). Benefit from the high sensitivity within a small strain range, the bladder can perceive the remote stimuli that are transmitted through water. Such a remote sensibility could further provide the fish a sufficient response time to inflate/deflate the bladder for avoiding dangers, enable it to detect or communicate with other organisms. For example, when a ball fell from a height of 20 cm around the bladder, the resistance presents a violent upward peak in real-time detection (Fig. 6b). Besides, with increasing the weight of the ball, the $\Delta R/R_0$ revealed a stronger oscillation (Fig. S12a). As a comparison, when the artificial swim bladder actuator was placed in the air, the corresponding vibration signal can't be detected. This phenomenon may be attributed to the following two reasons: 1) The attenuation of vibration propagation in solid-liquid is much lower than that in solid-gas, which causes the self-sensing actuator

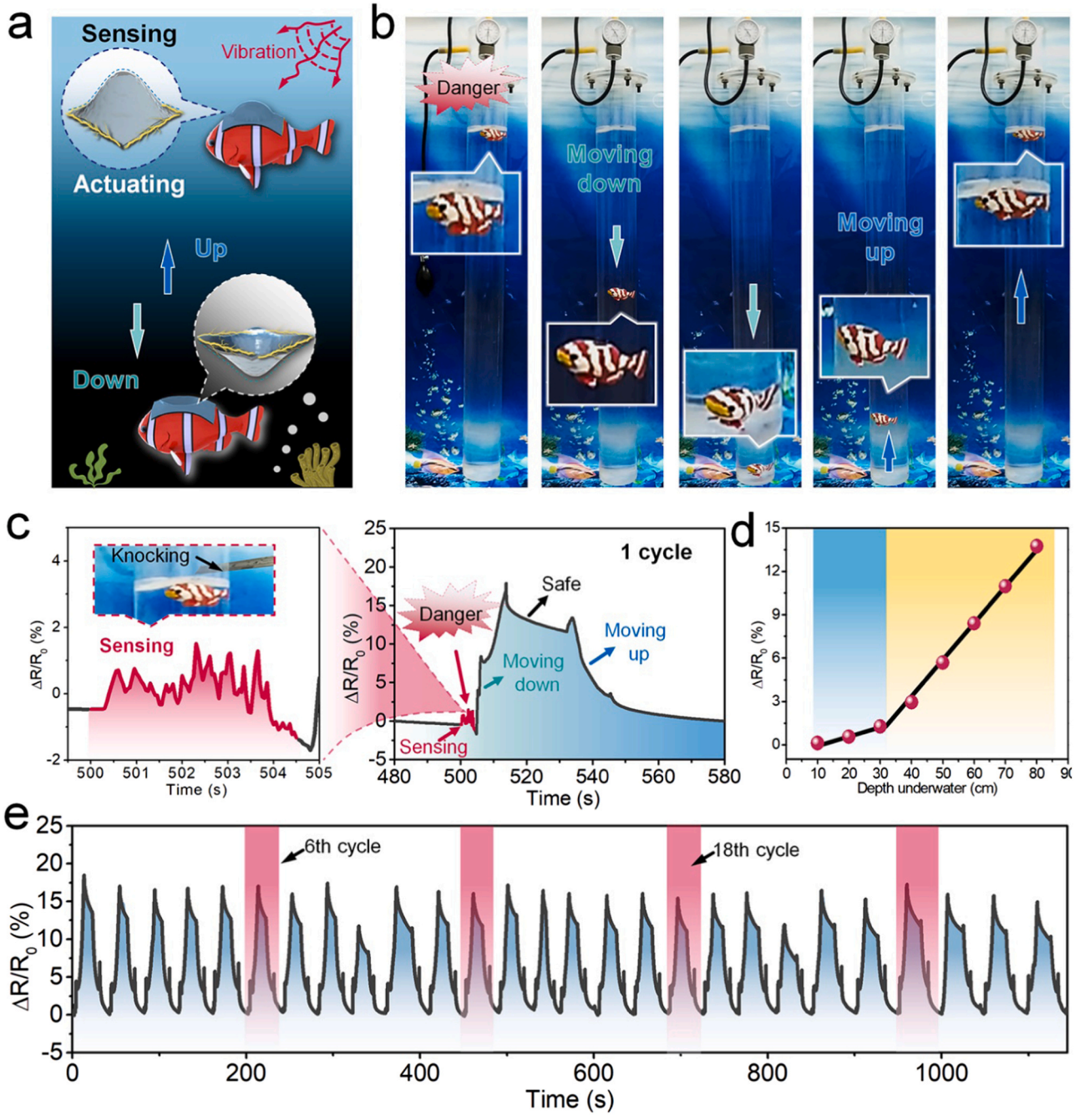

Fig. 7. (a) Schematic diagram of the artificial swim bladder pneumatic actuator. (b) Time-lapse images of the diving/surfacing process of the actuator. The direction of the arrows indicates the moving directions. (c) The artificial swim bladder pneumatic actuator is capable of sensing the dangerous vibration, guiding and tracing its further motions. (d) Perception of the underwater position of artificial swim bladder actuator. (e) A real-time signal record during the repetitive diving/surfacing process of the artificial swim bladder pneumatic actuator.

received a stronger vibration signal in the water. 2) When the vibration is transmitted to the medium, the arose vibrational medium will further cause the vibration of the sensor film. Owing to the larger density of the water than the air, the former will more easily cause the deformation of the film. Furthermore, when a ball (8.4 g) falls from different heights, the bladder behaves an increased response with falling height heighten (Figs 6c and S12b). Moreover, human activities including stomping (Figs 6d and S13a), stepping (Figs 6e and S13b), playing basketball (Figs 6f and S13c), knocking water container by a ruler (Figs 6g and S13d) can also be precisely detected by the artificial swim bladder.

Apart from excellent sensing ability to the vibrations from external activities, the waves that were directly generated in the water surface were also successfully detected. As depicted in Figs 6h and S13e in Supporting Information, when blowing air at the water surface, a responsive reversely sharp downward peak appeared and finally returned to peace in the real-time curve. The response of electric signals reveals a similar trend when stirring the water surface with a ruler (Figs 6i and S13f). These above results proved that the artificial swim bladder is of ultra-high sensitivity and stability in underwater detection, which shows the potential of constructing an integrated system of actuating and sensing.

Through the precise sensing of the surrounding environment, living organisms can guide their behaviors for self-protection, predation or communication. For example, a fish will swim away from danger to ensure self-protection after perceiving the danger signals (Fig. S14). We attempted to mimic these interesting behaviors as demonstrated by artificial swim bladder through integrating sensing and actuation functions (Fig. 7a). As a proof-of-concept, a hollow model fish actuator with a density of 0.998 g/cm^3 was put into an airtight container with water, and stayed at the water surface. When the container is knocked by a ruler as a danger, the danger signal can be detected by the actuator. According to the detected signal, a positive pressure was applied to the whole system. Then the PCP film sagged inward and dived to the bottom of the container to stay away from the danger source. After the actuator reached the bottom for a while and the danger signal disappeared, the actuator rose to the surface again, maintaining a comfortable and stable state, just like a real fish (Fig. 7b and c). Meanwhile, the electrical signal of the actuator can be recorded during the diving/surfacing motions process. Furthermore, the artificial swim bladder actuator enables to perceive the underwater position (Figs 7d and S15), due to the different water pressures caused by different depths. More importantly, the artificial swim bladder actuator shows excellent long-term stability, durability and reliability for tracking the repeatedly diving/surfacing processes (Fig. 7e). Even though immersed in water 6 months later, the morphology of the device still maintains a good state without breakage after suffering the durability test for 150 diving/surfacing cycles and the real-time variation of the resistance during the motions shows stable and continuous responses (Fig. S16). In this way, an artificial swim bladder pneumatic actuator with self-perception and signal feedback capabilities is demonstrated for the first time, paving the road for the next generation soft machines that are expected to be potentially useful to many different areas.

3. Conclusion

In conclusion, we develop a biomimetic artificial swim bladder pneumatic actuator via conformal sandwiched integrating enabled by synergetic locomotive a sensory soft materials system, in which the elastic conductive ultrathin film with sandwiched structures is deployed to effectively integrate the sensing and actuating features. The desirable morphable characteristic of the integrated film enables a reversible and controllable underwater locomotion. Owing to the alternative introduction of conductive CNTs film into the stretchable PDMS matrix, the sandwiched film endowed with the sensitive sensory function can effectively capture the underwater locomotive behavior to realize synergetic sensing and actuating integration. As a proof-of-concept, an artificial swim bladder integrated fish is designed to imitate the biomimetic behaviors. When dived into the water, the bionic fish can achieve real-time detection of the slight vibration signal from the internal/external environment and further be pneumatically actuated to escape from the dangerous areas. This work provides new insights into the design of integrated and intelligent soft systems for underwater synergetic locomotion and sensing behaviors.

4. Material and methods

4.1. Materials

The raw carbon nanotubes (CNTs) (diameter, about 20–30 nm; length, about 10–30 μm; -COOH %, about 1.23 wt%) with a purity of over 98% were purchased from Chengdu Organic Chemistry Co., Ltd., and were rinsed thoroughly with anhydrous ethanol and dried in a stream of nitrogen before use. PDMS with the weight ratio of base agent to curing agent 10:1 was fabricated from Sylgard 184 (Dowcorning, US). Other analytical reagent grade solvents and reagents were obtained from Sinopharm Chemical Reagent Co., Ltd. and used as received. The Milli-Q-grade water was used to prepared CNTs/PDMS Janus hybrid film at the air/water interface.

4.2. Preparation of CNTs film

The CNTs films at the air/water interface were prepared according to previous Langmuir-Blodgett assembled methods with some alterations. Typically, 200 mg of the pre-prepared CNTs were dispersed with 200 mL anhydrous ethanol, followed by strong ultrasonication for 2 h using an ultrasonic to form a stable dispersion. Subsequently, the resultant uniform CNTs dispersion was spread onto the water surface by a spray-coating method for the appropriate volume, and a uniform pre-assembled film formed at the air/water interface. Finally, after stabilized for about 30 min, the capillary substances like tissue or microporous sponges were selected to put on one side of the interface to quickly siphon water from the system, followed by a prominent decrease in the area of the preassembled CNTs film. Notably, the homogeneous preassembled CNTs layers were closely packed toward the opposite direction of the siphon situation. When the compression of the film stopped and further sponges could not compress the film, the resulting film was ultimately formed, indicating a closely packed structure.

4.3. Preparation of ultrathin PDMS and CNTs/PDMS Janus film

The PDMS base agent and curing agent with weight ratio 10:1 was diluted using N-heptane with a weight ratio of 4%. The obtained mixture solution ($\approx$ 1500 mL/m^2) was sprayed onto the surface of the as-prepared CNTs film or sprayed onto the water surface. After the N-heptane volatilized completely, the prepared film was transferred to the oven with temperature 70 °C for 2 h and the CNTs/PDMS ultrathin Janus film and PDMS film with thickness ~ 30 μm obtained at air/water interface.

4.4. Fabrication of the artificial swim bladder pneumatic actuators

First, the model fish (50 × 48.5 × 26.3 mm^3 with an elliptical hole of 16 × 11 cm^2 at the back) was prepared from commercially polylactic acid (PLA) through 3D printing. The density of the PLA alone is about 1.25 g/cm^3. Then, the as-prepared CNTs/PDMS ultrathin Janus film was transferred onto the hole of the mode fish with coated uncured PDMS mixture, when it completely dried at room temperature the conductive copper wires were connected at the two sides of the hole with silver paste. Next, another encapsulating PDMS layer was transferred onto the CNTs/PDMS ultrathin Janus film surface. Finally, the uncuring PDMS mixture was further coated on the edge of the film to ensure completely sealed.

4.5. Characterization

Scanning electron microscopy (SEM) was performed to observe the micromorphology of CNTs/PDMS Janus hybrid film with a Hitachi S-4800 cold field emission SEM at an accelerating voltage of 8 kV. Raman spectra were collected by R-3000HR spectrometer (Raman Systems, Inc., R-3000 series) using a solid-state diode laser (532 nm) as an excitation source with a frequency range of 3500–300 cm^{-1}. When characterization of the sensing performance of the CNTs/PDMS Janus film, an Instron 5567 universal testing machine was used to stretch CNTs/PDMS rectangular specimens (25 mm × 3 mm) with one end fixed and the other end linearly elongated at a constant speed. Resistance measurements were carried out by connecting the two ends of the CNTs/PDMS Janus hybrid film to an Electrochemical Workstation (CH Instruments, CHI660E.Chenhua Co., Shanghai, China), with conductive copper wires to record the real-time current (I) flowing through the film under a constant voltage (U_0) of 1 V, while the real-time resistance (R) was calculated by the equation $R = U_0/I$. The fish mode was printed by using a commercial Polyjet multi-material 3D printer (A4S, JGARORA Ltd., Shenzhen, China). Photographic images were taken with an MIUI 6X smartphone. The positive pressure and negative pressure were collective by sphygmomanometer and pressure gage, respectively.

CRediT authorship contribution statement

Yun Liang: Conceptualization, Methodology, Data curation, Writing original draft, Writing - review & editing. **Peng Xiao**: Conceptualization, Methodology, Writing - review & editing, Resources, Supervision. **Feng Ni**: Data curation. **Ling Zhang**: Methodology, Writing - review & editing. **Tao Zhang**: Validation, Writing - review & editing. **Shuai Wang**: Data curation. **Wei Zhou**: Data curation. **Wei Lu**: Suggestion, Resources. **Shiao-Wei Kuo**: Resources. **Tao Chen**: Conceptualization, Writing - review & editing, Resources, Supervision.

Declaration of Competing Interest

The authors declare that they have no known competing financial interests or personal relationships that could have appeared to influence the work reported in this paper.

Acknowledgements

We thank the Natural Science Foundation of China (52073295, 51803226, 51773214), Key Research Program of Frontier Sciences, Chinese Academy of Sciences (QYZDB-SSWSLH036), Bureau of International Cooperation, Chinese Academy of Sciences (174433KYSB20170061), Postdoctoral Innovation Talent Support Program (BX20180321), China Postdoctoral Science Foundation (2018M630695) and Ningbo Scientific and Technological Innovation 2025 Major Project (2018B10057).

Appendix A. Supporting information

Supplementary data associated with this article can be found in the online version at doi:10.1016/j.nanoen.2020.105617.

References

[1] S. Kim, C. Laschi, B. Trimmer, Soft robotics: a bioinspired evolution in robotics, Trends Biotechnol. 31 (5) (2013) 287–294.
[2] P. Polygerinos, N. Correll, S.A. Morin, B. Mosadegh, C.D. Onal, K. Petersen, M. Cianchetti, M.T. Tolley, R.F. Shepherd, Soft robotics: review of fluid-driven intrinsically soft devices; manufacturing, sensing, control, and applications in human-robot interaction, Adv. Eng. Mater. 19 (12) (2017), 1700016.
[3] F. Fu, L. Shang, Z. Chen, Y. Yu, Y. Zhao, Bioinspired living structural color hydrogels, Sci. Robot. 3 (16) (2018) eaar8580.
[4] S. Wei, W. Lu, X. Le, C. Ma, H. Lin, B. Wu, J. Zhang, P. Theato, T. Chen, Bioinspired synergistic fluorescence-color-switchable polymeric hydrogel actuators, Angew. Chem. Int. Ed. 58 (45) (2019) 16243–16251.
[5] J. Mu, G. Wang, H. Yan, H. Li, X. Wang, E. Gao, C. Hou, A.T.C. Pham, L. Wu, Q. Zhang, Y. Li, Z. Xu, Y. Guo, E. Reichmanis, H. Wang, M. Zhu, Molecular-channel driven actuator with considerations for multiple configurations and color switching, Nat. Commun. 9 (1) (2018) 590.
[6] C. Larson, B. Peele, S. Li, S. Robinson, M. Totaro, L. Beccai, B. Mazzolai, R. Shepherd, Highly stretchable electroluminescent skin for optical signaling and tactile sensing, Science 351 (6277) (2016) 1071–1074.
[7] Y. Gu, X. Wang, W. Gu, Y. Wu, T. Li, T. Zhang, Flexible electronic eardrum, Nano Res. 10 (8) (2017) 2683–2691.
[8] Y. Hu, J. Liu, L. Chang, L. Yang, A. Xu, K. Qi, P. Lu, G. Wu, W. Chen, Y. Wu, Electrically and sunlight-driven actuator with versatile biomimetic motions based on rolled carbon nanotube bilayer composite, Adv. Funct. Mater. 27 (44) (2017), 1704388.
[9] M. Zhang, Y. Wang, M. Jian, C. Wang, X. Liang, J. Niu, Y. Zhang, Spontaneous alignment of graphene oxide in hydrogel during 3D printing for multistimuli-responsive actuation, Adv. Sci. 7 (6) (2020), 1903048.
[10] Y.L. Park, B.R. Chen, N.O. Perez-Arancibia, D. Young, L. Stirling, R.J. Wood, E. C. Goldfield, R. Nagpal, Design and control of a bio-inspired soft wearable robotic device for ankle-foot rehabilitation, Bioinspir. Biomim. 9 (1) (2014), 016007.
[11] S. Bauer, S. Bauer-Gogonea, I. Graz, M. Kaltenbrunner, C. Keplinger, R. Schwodiauer, 25th anniversary article: a soft future: from robots and sensor skin to energy harvesters, Adv. Mater. 26 (1) (2014) 149–161.
[12] Y. Cheng, R. Wang, K.H. Chan, X. Lu, J. Sun, G.W. Ho, A biomimetic conductive tendril for ultrastretchable and integratable electronics, muscles, and sensors, ACS Nano 12 (4) (2018) 3898–3907.
[13] R. Dahiya, N. Yogeswaran, F. Liu, L. Manjakkal, E. Burdet, V. Hayward, H. Jorntell, Large-area soft e-skin: the challenges beyond sensor designs, Proc. IEEE 107 (10) (2019) 2016–2033.
[14] T. Li, Y. Li, T. Zhang, Materials, structures, and functions for flexible and stretchable biomimetic sensors, Acc. Chem. Res. 52 (2) (2019) 288–296.
[15] C. Wang, K. Xia, H. Wang, X. Liang, Z. Yin, Y. Zhang, Advanced carbon for flexible and wearable electronics, Adv. Mater. 31 (9) (2018) 1801072–1801108.
[16] M. Jian, K. Xia, Q. Wang, Z. Yin, H. Wang, C. Wang, H. Xie, M. Zhang, Y. Zhang, Flexible and highly sensitive pressure sensors based on bionic hierarchical structures, Adv. Funct. Mater. 27 (9) (2017), 1606066.
[17] S.A. Morin, R.F. Shepherd, S.W. Kwok, A.A. Stokes, A. Nemiroski, G.M. Whitesides, Camouflage and display for soft machines, Science 337 (6096) (2012) 828–832.
[18] J.H. Pikul, S. Li, H. Bai, R.T. Hanlon, I. Cohen, R.F. Shepherd, Stretchable surfaces with programmable 3D texture morphing for synthetic camouflaging skins, Science 358 (6360) (2017) 210–214.
[19] E. Acome, S.K. Mitchell, T.G. Morrissey, M.B. Emmett, C. Benjamin, M. King, M. Radakovitz, C. Keplinger, Hydraulically amplified self-healing electrostatic actuators with muscle-like performance, Science 359 (6371) (2018) 61–65.
[20] H. Yuk, S. Lin, C. Ma, M. Takaffoli, N.X. Fang, X. Zhao, Hydraulic hydrogel actuators and robots optically and sonically camouflaged in water, Nat. Commun. 8 (2017) 14230.
[21] T. Arnold, M. Scheutz, The tactile ethics of soft robotics: designing wisely for human-robot interaction, Soft Robot. 4 (2) (2017) 81–87.
[22] M. Wehner, R.L. Truby, D.J. Fitzgerald, B. Mosadegh, G.M. Whitesides, J.A. Lewis, R.J. Wood, An integrated design and fabrication strategy for entirely soft, autonomous robots, Nature 536 (7617) (2016) 451–455.
[23] J. Shintake, V. Cacucciolo, D. Floreano, H. Shea, Soft robotic grippers, Adv. Mater. 30 (2018), 1707035.
[24] Y. Yang, Y. Wu, C. Li, X. Yang, W. Chen, Flexible actuators for soft robotics, Adv. Intell. Syst. 2 (1) (2019), 1900077.
[25] K.B. Justus, T. Hellebrekers, D.D. Lewis, A. Wood, C. Ingham, C. Majidi, P. R. LeDuc, C. Tan, A biosensing soft robot: autonomous parsing of chemical signals through integrated organic and inorganic interfaces, Sci. Robot. 4 (31) (2019) eaax0765.
[26] T.G. Thuruthel, B. Shih, C. Laschi, M.T. Tolley, Soft robot perception using embedded soft sensors and recurrent neural networks, Sci. Robot. 4 (26) (2019) eaav1488.
[27] R.L. Truby, M. Wehner, A.K. Grosskopf, D.M. Vogt, S.G.M. Uzel, R.J. Wood, J. A. Lewis, Soft somatosensitive actuators via embedded 3D printing, Adv. Mater. 30 (15) (2018), 1706383.
[28] B. Shih, D. Shah, J. Li, T.G. Thuruthel, Y.-L. Park, F. Iida, Z. Bao, R. Kramer-Bottiglio, M.T. Tolley, Electronic skins and machine learning for intelligent soft robots, Sci. Robot. 5 (2020) eaaz9239.
[29] H. Zhao, K. O'Brien, S. Li, R. Shepherd, Optoelectronically innervated soft prosthetic hand via stretchable optical waveguides, Sci. Robot. 1 (1) (2016) eaai7529.
[30] C.Y. Qu, S.Q. Wang, L. Liu, Y.Y. Bai, L.H. Li, F.Q. Sun, M.M. Hao, T. Li, Q.F. Lu, L. L. Li, S.J. Qin, T. Zhang, Bioinspired flexible volatile organic compounds sensor based on dynamic surface wrinkling with dual-signal response, Small 15 (17) (2019), 1900216.
[31] C. Xu, M. Colorado Escobar, A.A. Gorodetsky, Stretchable cephalopod-inspired multimodal camouflage systems, Adv. Mater. 32 (16) (2020), 1905717.
[32] Y. Hu, G. Wu, T. Lan, J. Zhao, Y. Liu, W. Chen, A graphene-based bimorph structure for design of high performance photoactuators, Adv. Mater. 27 (47) (2015) 7867–7873.
[33] L. Yang, L. Chang, Y. Hu, M. Huang, Q. Ji, P. Lu, J. Liu, W. Chen, Y. Wu, An autonomous soft actuator with light-driven self-sustained wavelike oscillation for

phototactic self-locomotion and power generation, Adv. Funct. Mater. 30 (15) (2020), 1908842.
[34] T. Cheng, G. Li, Y. Liang, M. Zhang, B. Liu, T.-W. Wong, J. Forman, M. Chen, G. Wang, Y. Tao, T. Li, Untethered soft robotic jellyfish, Smart Mater. Struct. 28 (1) (2019), 015019.
[35] T.F. Li, G.R. Li, Y.M. Liang, T.Y. Cheng, J. Dai, X.X. Yang, B.Y. Liu, Z.D. Zeng, Z. L. Huang, Y.W. Luo, T. Xie, W. Yang, Fast-moving soft electronic fish, Sci. Adv. 3 (4) (2017), e1602045.
[36] J.L. Finney, G.N. Robertson, C.A. McGee, F.M. Smith, R.P. Croll, Structure and autonomic innervation of the swim bladder in the zebrafish (Danio rerio), J. Comp. Neurol. 495 (5) (2006) 587–606.
[37] R.A. Mohr, E.A. Whitchurch, R.D. Anderson, P.M. Forlano, R.R. Fay, D.R. Ketten, T. C. Cox, J.A. Sisneros, Intra- and Intersexual swim bladder dimorphisms in the plainfin midshipman fish (Porichthys notatus): implications of swim bladder proximity to the inner ear for sound pressure detection, J. Morphol. 278 (11) (2017) 1458–1468.
[38] K.S. Boyle, S. Riepe, G. Bolen, E. Parmentier, Variation in swim bladder drumming sounds from three doradid catfish species with similar sonic morphologies, J. Exp. Biol. 218 (Pt 18) (2015) 2881–2891.
[39] M. Song, M. Cheng, M. Xiao, L. Zhang, G. Ju, F. Shi, Biomimicking of a swim bladder and its application as a mini-generator, Adv. Mater. 29 (7) (2017) 1603312–1603315.
[40] A. Hamidi, Y. Almubarak, Y.M. Rupawat, J. Warren, Y. Tadesse, Poly-Saora robotic jellyfish: swimming underwater by twisted and coiled polymer actuators, Smart Mater. Struct. 29 (4) (2020), 045039.
[41] S. Wang, B. Huang, D. McCoul, M. Li, L. Mu, J. Zhao, A soft breaststroke-inspired swimming robot actuated by dielectric elastomers, Smart Mater. Struct. 28 (4) (2019), 045006.
[42] J. Shintake, V. Cacucciolo, H. Shea, D. Floreano, Soft biomimetic fish robot made of dielectric elastomer actuators, Soft Robot. 5 (4) (2018) 466–474.
[43] R.H. Crawford, Structure of an air-breathing organ and the swim bladder in the Alaska blackfish, Dallia pectoralis Bean, Can. J. Zool. 52 (1974) 1221–1225.
[44] P. Xiao, Y. Liang, J. He, L. Zhang, S. Wang, J. Gu, J. Zhang, Y. Huang, S.W. Kuo, T. Chen, Hydrophilic/hydrophobic interphase-mediated bubble-like stretchable Janus ultrathin films toward self-adaptive and pneumatic multifunctional electronics, ACS Nano 13 (4) (2019) 4368–4378.
[45] P. Xiao, J. Gu, C. Wan, S. Wang, J. He, J. Zhang, Y. Huang, S.-W. Kuo, T. Chen, Ultrafast formation of free-standing 2D carbon nanotube thin films through capillary force driving compression on an air/water interface, Chem. Mater. 28 (19) (2016) 7125–7133.
[46] Z. Liu, H. Wang, P. Huang, J. Huang, Y. Zhang, Y. Wang, M. Yu, S. Chen, D. Qi, T. Wang, Y. Jiang, G. Chen, G. Hu, W. Li, J. Yu, Y. Luo, X.J. Loh, B. Liedberg, G. Li, X. Chen, Highly stable and stretchable conductive films through-thermal-radiation-assisted metal encapsulation, Adv. Mater. 31 (35) (2019), 1901360.
[47] M. Amjadi, A. Pichitpajongkit, S. Lee, S. Ryu, I. Park, Highly stretchable and sensitive strain sensor based on silver nanowire-elastomer nanocomposite, ACS Nano 8 (2014) 5154–5163.
[48] S. Xu, Z. Fan, C. Li, P. Wang, K.A. Sammed, L. Pan, Investigation of strain sensing mechanisms on ultra-thin carbon nanotube networks with different densities, Carbon 155 (2019) 421–431.
[49] B. Hu, N. Hu, Y. Li, K. Akagi, W. Yuan, T. Watanabe, Y. Cai, Multi-scale numerical simulations on piezoresistivity of CNT/polymer nanocomposites, Nanoscale Res. Lett. 7 (1) (2012) 402–412.
[50] L. Wang, Y. Chen, L. Lin, H. Wang, X. Huang, H. Xue, J. Gao, Highly stretchable, anti-corrosive and wearable strain sensors based on the PDMS/CNTs decorated elastomer nanofiber composite, Chem. Eng. J. 362 (2019) 89–98.
[51] W.S. Lee, D. Kim, B. Park, H. Joh, H.K. Woo, Y.-K. Hong, T.-i Kim, D.-H. Ha, S. J. Oh, Multiaxial and transparent strain sensors based on synergetically reinforced and orthogonally cracked hetero-nanocrystal solids, Adv. Funct. Mater. 29 (4) (2019), 1806714.
[52] D. Jiang, Y. Wang, B. Li, C. Sun, Z. Wu, H. Yan, L. Xing, S. Qi, Y. Li, H. Liu, W. Xie, X. Wang, T. Ding, Z. Guo, Flexible sandwich structural strain sensor based on silver nanowires decorated with self-healing substrate, Macromol. Mater. Eng. 304 (7) (2019), 1900074.
[53] T. Yamada, Y. Hayamizu, Y. Yamamoto, Y. Yomogida, A. Izadi-Najafabadi, D. N. Futaba, K. Hata, A stretchable carbon nanotube strain sensor for human-motion detection, Nat. Nanotechnol. 6 (5) (2011) 296–301.
[54] C. Yan, J. Wang, W. Kang, M. Cui, X. Wang, C.Y. Foo, K.J. Chee, P.S. Lee, Highly stretchable piezoresistive graphene-nanocellulose nanopaper for strain sensors, Adv. Mater. 26 (13) (2014) 2022–2027.
[55] J. Lee, M. Lim, J. Yoon, M.S. Kim, B. Choi, D.M. Kim, D.H. Kim, I. Park, S.J. Choi, Transparent, flexible strain sensor based on a solution-processed carbon nanotube network, ACS Appl. Mater. Interfaces 9 (31) (2017) 26279–26285.
[56] F. Yuan, S. Wang, S. Zhang, Y. Wang, S. Xuan, X. Gong, A flexible viscoelastic coupling cable with self-adapted electrical properties and anti-impact performance toward shapeable electronic devices, J. Mater. Chem. C 7 (27) (2019) 8412–8422.
[57] Y. Wang, Y. Jia, Y. Zhou, Y. Wang, G. Zheng, K. Dai, C. Liu, C. Shen, Ultra-stretchable, sensitive and durable strain sensors based on polydopamine encapsulated carbon nanotubes/elastic bands, J. Mater. Chem. C 6 (30) (2018) 8160–8170.
[58] B.-U. Hwang, J.-H. Lee, T.Q. Trung, E. Roh, D.-I. Kim, S.-W. Kim, N.-E. Lee, Transparent stretchable self-powered patchable sensor platform with ultrasensitive recognition of human activities, ACS Nano 9 (9) (2015) 8801–8810.
[59] D.Y. Wang, L.Q. Tao, Y. Liu, T.Y. Zhang, Y. Pang, Q. Wang, S. Jiang, Y. Yang, T. L. Ren, High performance flexible strain sensor based on self-locked overlapping graphene sheets, Nanoscale 8 (48) (2016) 20090–20095.
[60] M. Amjadi, M. Sitti, Self-sensing paper actuators based on graphite-carbon nanotube hybrid films, Adv. Sci. 5 (7) (2018), 1800239.
[61] X. Yang, M. Cheng, L. Zhang, S. Zhang, X. Liu, F. Shi, Electricity generation through light-responsive diving-surfacing locomotion of a functionally cooperating smart device, Adv. Mater. 30 (36) (2018) 1803125–1803130.
[62] M. Song, M. Cheng, M. Xiao, L. Zhang, G. Ju, F. Shi, Biomimicking of a swim bladder and its application as a mini-generator, Adv. Mater. 29 (7) (2017) 1603312–1603315.

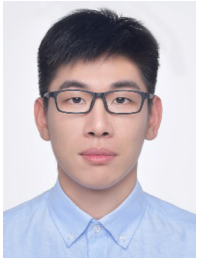

Yun Liang received his B.S. degree from Southwest University of Science and Technology. Currently, He is a Ph.D. student in the Ningbo Institute of Materials Technology and Engineering, Chinese Academy of Sciences, under the supervision Professor Tao Chen. His current research interests focus on polymer/Carbon-based 2D hybrid materials and their applications as sensors and actuators.

Dr. Peng Xiao received his Ph.D. in polymer chemistry and physics from Ningbo Institute of Materials Technology and Engineering, Chinese Academy of Sciences in 2017, under the supervision of Prof. Tao Chen. After that he joint Tao Chen's group as a postdoctoral research fellow. His current research interest focuses on the macroscopic self-assembly of 1D and 2D of carbon-based nanomaterials into 2D ultrathin films at air/water interface and further interfacial asymmetric modification to explore their potential applications in actuators, sensors and solar-to-thermal conversion.

Feng Ni received his B.S. degree from Tianjin Polytechnic University in 2017. Currently, he is a Ph.D. student in the Ningbo Institute of Materials Technology and Engineering, Chinese Academy of Sciences, under the supervision Professor Tao Chen. His current research interests focus on polymer/carbon-based 2D hybrid materials and photo-thermal conversion.

Ling Zhang received her MS degree of chemistry engineering from Ningbo Institute of Materials Technology and Engineering, Chinese Academy of Sciences in 2020. Currently, she is a Ph.D. candidate in the University of Manchester, under the supervision of Prof. Wuliang Yin. Her research interests focus on the integration of textile-based electronics with the interdiscipline of materials science and electronics engineering.

Prof. Tao Zhang is a full professor at Ningbo Institute of Materials Technology and Engineering, Chinese Academy of Sciences since 2020. He received his Ph.D. degree in polymer chemistry under the supervision of Prof. Rainer Jordan from Technische Universitat Dresden (Germany) in 2015. Then, he worked in Prof. Xiniang Feng's group as a postdoctoral researcher at Technische Universitat Dresden (2016–2019). His current research interest focuses on design and synthesis polymer thin films (in solution/at interfaces) such as polymer brushes, 2D polymers, 2D COFs, and 2D MOFs as well as their applications in functional coatings and devices.

Dr. Shuai Wang received his Ph.D. in polymer chemistry and physics from Ningbo Institute of Materials Technology and Engineering, Chinese Academy of Sciences in 2019, under the supervision of Prof. Tao Chen. His current research interests focus on the construction of carbon-based nanomaterials and polymer hybrid materials and exploring their potential applications in wearable strain sensors, programmable soft robotics, multifunctional integrated device, etc.

Wei Zhou received his B.S. degree from Harbin Engineering University in 2019. Now, he is a Ph.D. student in the Ningbo Institute of Materials Technology and Engineering, Chinese Academy of Sciences, under the supervision of Professor Tao Chen. His current research interests focus on the construction of carbon-based hybrid materials and their applications in flexible sensors.

Prof. Wei Lu received his Ph.D. degree in polymer chemistry and physics from Zhejiang University in China (2014). Soon afterwards he joined Ningbo Institute of Materials Technology and Engineering, Chinese Academy of Sciences. He was promoted to Associate Professor in 2017 and Professor in 2020. His current research is focused on the fabrication of luminescent polymeric materials for applications in chemical sensing and biomimetic actuators.

Prof. Shiao-Wei Kuo received his B.Sc. in chemical engineering from the National Chung Hsing University (1998) and Ph. D. in applied chemistry from the National Chiao Tung University in Taiwan (2002). He continued his research work at Chiao Tung University as a postdoctoral researcher during 2002–2007. Now, he is the professor in the Department of Materials and Optoelectronic Science, National Sun Yat-Sen University, Taiwan. His research interests include polymer interactions, self-assembly nanostructures, covalent organic frameworks, porous materials, POSS nanocomposites, polybenzoxazine, and polypeptides.

Prof. Tao Chen received his Ph.D. in polymer chemistry and physics from Zhejiang University in 2006. After his postdoctoral training at the University of Warwick (UK), he joined Duke University (USA) as a research scientist. He then moved back to Europe as an Alexander von Humboldt Research Fellow at Technische Universität Dresden, Germany. Since 2012, he is a full-time professor at Ningbo Institute of Materials Technology and Engineering, Chinese Academy of Sciences. His research interests include smart polymers and their hybrid systems with applications as actuators, shape memory polymers, and chemical sensing.